Constrained Optimal Control of the Step-down DC-DC Converter

Tobias Geyer, *Member, IEEE*, Georgios Papafotiou, *Member, IEEE*, Roberto Frasca, *Member, IEEE*, and Manfred Morari, *Fellow, IEEE*

Abstract

In this paper, we propose a novel approach to the modelling and controller design of the synchronous step-down dc-dc converter. We introduce a hybrid converter model that is valid for the whole operating regime and captures the different modes of operation. Based on this model, we formulate and solve a constrained optimal control problem. This allows a systematic controller design that achieves the regulation of the output voltage to its reference despite input voltage and output load variations while satisfying the constraints on the duty cycle and the inductor current. The resulting state-feedback control law is of piecewise affine form, which can be easily stored and implemented in a look-up table. A Kalman filter is added to account for unmeasured load variations and to achieve zero steady-state output voltage error. Experimental results demonstrate the potential advantages of the proposed control methodology.

I. Introduction

Nowadays, switch-mode dc-dc conversion is a mature and well-established technology used in a large variety of demanding applications. Yet, the control problems associated with such converters still pose theoretical and practical challenges, which manifest themselves in the numerous publications on this subject over the last years. The development of advanced control techniques together with the increased computational power of the available hardware in the control loop allow tackling the control problem from a new perspective. In this paper, we propose a new approach to the problem – namely, we pose and solve the constrained optimal control problem for fixed-frequency switch-mode dc-dc converters.

The difficulties in controlling dc-dc converters arise from their hybrid nature. In general, these converters feature three different modes of operation, where each mode has an associated linear continuous-time dynamic. Furthermore, constraints are present, which result from the converter topology. In particular, the manipulated variable (the duty cycle) is bounded between zero and one, and in the discontinuous current operation a state

This work was done at the Automatic Control Laboratory, ETH Zurich, Switzerland. T. Geyer is currently with GE Global Research Europe, Munich, Germany, tobias.geyer@research.ge.com; G. Papafotiou is now with ABB Corporate Research, Dättwil, Switzerland, georgios.papafotiou@ch.abb.com; R. Frasca is with the Department of Engineering, Università del Sannio, Benevento, Italy, frasca@unisannio.it; M. Morari is with the Automatic Control Laboratory, ETH Zurich, Switzerland, morari@control.ee.ethz.ch.

Correspondence to: Tobias Geyer, GE Global Research Europe, Freisinger Landstr. 50, 85748 Garching b. Munich, Germany, tel +49 89 5528 3435, fax +49 89 5528 3180, tobias.geyer@research.ge.com

Part of this work has been previously presented in the 2004 IEEE Workshop on Computers in Power Electronics (COMPEL), Champaign, IL, USA, August 2004.

(inductor current) is constrained to be nonnegative. Additional constraints may be imposed as safety measures, such as current limiting or soft-starting, where the latter constitutes a constraint on the maximal derivative of the current during start-up. The control problem is further complicated by gross changes in the operating point that occur due to input voltage and output load variations.

The dominant approach to the modelling and controller design of switch-mode dc-dc converters is the method of state-space averaging [1], [2] and the design of a control loop comprising a PI-type controller and a Pulse Width Modulation (PWM) unit. The controller is tuned for a model locally linearized around a specific operating point. In the literature a wide range of strategies have been proposed for improving the controller design, but the majority of the proposed design methods is still based on averaged and/or locally linearized models of the converters. In this category, the methods introduced vary from Fuzzy Logic [3] to Linear Quadratic Regulators (LQR) [4], and from non-linear control techniques [5], [6], [7] to feedforward control [8], [9].

Due to space limitations, we provide here only a brief overview of the literature most related to our approach – a more extensive coverage can be found in Section 8.1.2 of [10]. In [11], [12], the authors propose an (unconstrained) LQR controller based on a locally linearized discrete-time model of the averaged dc-dc converter. In [13], an unconstrained nonlinear predictive controller is formulated for a dc-dc converter using a control methodology that extends the concept of Generalized Predictive Control [14] to nonlinear systems. For the latter, an implementation may prove to be difficult due to the lack of convergence guarantees and the potentially excessive computation time. As an unconstrained optimization problem is solved, the constraints on the duty cycle and the inductor current cannot be handled in a straightforward manner.

More recently, the research effort has also focused on digital control techniques, enabled by the rapid evolution of the available control hardware. As examples, the reader is referred to [15] and [16] for digital control techniques applied to dc-dc converters, and to [17] and [18] for a presentation of the related frequency domain modelling and an analysis of the issues stemming from the digital quantization effects, respectively. Furthermore, predictive digital control techniques have also been reported for the case of power factor correction, see e.g. [19] for details.

Motivated by the aforementioned difficulties, we present a novel approach to the modelling and controller design problem for fixed-frequency dc-dc converters, using a synchronous step-down converter as an illustrative example. The converter is modelled as a hybrid system by deriving a piecewise affine (PWA) model that is valid for the whole operating range and captures the evolution of the state variables within the switching period. Based on the hybrid model, we formulate a constrained finite time optimal control problem, which is solved off-line using Dynamic Programming [20]. This approach leads to a state-feedback controller that is defined over the whole state-space and yields the duty cycle as a PWA function of the states. This controller can be considered as an extension of the LQR methodology (which is applicable to linear models only) to nonlinear (PWA) models. However, the most important feature is that such a controller can be implemented as a look-up table, thus avoiding the need for any on-line optimization. We would like to emphasize that the controller is designed such that for the control computation (which is effectively a look-up table evaluation) only directly available quantities are needed. In particular, we assume that – in accordance with common practice – the input voltage, the inductor current and the output voltage can be directly measured. In accordance with the digital

control methodology, all measurement and control actions take place only at the sampling instances, i.e at the beginning of the switching period.

The proposed approach carries several benefits – the most prominent being the systematic character of the design procedure that avoids excessive iterations and tuning. In particular, the control objectives are expressed in the cost function of the optimal controller in a straightforward manner, and all constraints are directly included in the design procedure leading to a controller that achieves current limiting without adopting the traditional implementation. Most importantly, the control law captures the whole operating regime due to the fact that the derived PWA model provides an accurate representation of the converter for the whole operating range. This leads to a favorable closed-loop performance that is independent from the operating point. Furthermore, the proposed control scheme rejects gross disturbances in the (measured) input voltage and the (unmeasured) load resistance.

These benefits, however, come at a cost. The derived controller is rather complex and the look-up table can easily comprise 50 or more entries. In some applications this may prove to be a limiting factor. Yet, the main scope of this paper is to illustrate that the application of advanced hybrid optimal control methods for dc-dc converters is conceivable and within reach. This is confirmed by the experimental results obtained. Moreover, compared with only locally valid controllers, a more complex solution is to be expected since the control problem is addressed for the complete operating regime.

The paper is organized as follows. Section II summarizes the nonlinear continuous-time state-space equations of the converter. The ν-resolution modelling approach, which yields a discrete-time hybrid converter model, is introduced and analyzed in Section III. Based on this model, we formulate and solve a constrained finite time optimal control problem in Section IV. Experimental results in Section V illustrate various aspects of the system's behavior, including start-up and gross changes in the input voltage and the load resistance. The paper is summarized in Section VI, where conclusions are also drawn.

II. Mathematical Model of Synchronous Converter

We start by modelling the physical behavior of the synchronous step-down converter in continuous time and derive for each mode of operation the state-space equations. This model will serve later as starting point for obtaining a model for controller design.

The circuit topology of the converter is shown in Fig. 1, where R_o denotes the output load, which we assume to be ohmic, R_c is the Equivalent Series Resistance (ESR) of the capacitor, R_ℓ is the internal resistance of the inductor, L and C represent the inductance and the capacitance of the low-pass filtering stage, respectively, and V_s denotes the input voltage. The semiconductor switches S_1 and S_2, which are operated dually, are driven by a pulse sequence with a constant switching frequency f_s (with period T_s). The duty cycle d is defined by $d = \frac{t_{on}}{T_s}$, where t_{on} represents the interval within the switching period during which the primary switch is in conduction. For every switching period k the duty cycle $d(k) \in [0, 1]$ is chosen by the controller.

We define $X(t) = [I_\ell(t)\ V_c(t)]^T$ as the state vector, where $I_\ell(t)$ is the inductor current and $V_c(t)$ the capacitor voltage. Given the duty cycle $d(k)$ during the k-th period, the system is described by the following set of affine

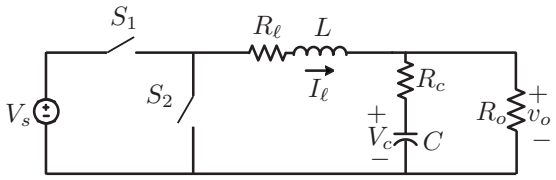

Fig. 1: Topology of the step-down synchronous converter

continuous-time state-space equations. While S_1 is conducting, they are given by

$$\frac{\mathrm{d}X(t)}{\mathrm{d}t} = FX(t) + fV_s, \quad kT_s \leqslant t < (k + d(k))T_s\,, \tag{1}$$

and when S_1 is off, the system evolves autonomously according to

$$\frac{\mathrm{d}X(t)}{\mathrm{d}t} = FX(t), \quad (k + d(k))T_s \leqslant t < (k + 1)T_s\,, \tag{2}$$

where the matrices F and f are given by

$$F = \begin{bmatrix} -\frac{1}{L}(R_\ell + \frac{R_o R_c}{R_o + R_c}) & -\frac{1}{L}\frac{R_o}{R_o + R_c} \\ \frac{1}{C}\frac{R_o}{R_o + R_c} & -\frac{1}{C}\frac{1}{R_o + R_c} \end{bmatrix} \tag{3}$$

and

$$f = \begin{bmatrix} \frac{1}{L} \\ 0 \end{bmatrix}, \tag{4}$$

respectively. The output voltage $V_o(t)$ across the load R_o is expressed as a function of the states through

$$V_o(t) = g^T X(t) \tag{5}$$

with

$$g = \begin{bmatrix} \frac{R_o R_c}{R_o + R_c} & \frac{R_o}{R_o + R_c} \end{bmatrix}^T. \tag{6}$$

Of main interest from a control point of view is the output voltage error

$$V_{o,err}(k) = \frac{1}{T_s}\int_{kT_s}^{(k+1)T_s} (V_o(t) - V_{o,ref})\,dt \tag{7}$$

integrated over the k-th switching period, where $V_{o,ref}$ denotes the reference of the output voltage.

The converter model includes constraints. By definition, the duty cycle $d(k)$ is constrained between zero and one. Moreover, a current limiting constraint has to be accounted for, which is given by $-I_{\ell,max} < I_\ell(t) < I_{\ell,max}$.

III. Modelling for Controller Design

In the following, we derive a model to serve as prediction model for the optimal control problem formulation in Section IV. For this, we reformulate the above presented converter model and introduce the ν-resolution modelling approach.

A. Normalization and Reformulation

First, to obtain a numerically suitable model for controller design, the converter equations are normalized. This is done by using the switching frequency, the nominal load resistance and the measured input voltage as base quantities. From these, the base current, base capacitance and base inductance can be deduced straightforwardly (see the Appendix for details). Second, from an implementation point of view, it is preferable that all states are directly measureable. Thus, in the state vector we replace the capacitor voltage by the output voltage[1].

Using the normalized and measureable state vector $x(t) = [i_\ell(t)\ v_o(t)]^T$, the system equations are rewritten as

$$\frac{\mathrm{d}x(t)}{\mathrm{d}t} = \begin{cases} Fx(t) + f, & kT_s \leqslant t < (k + d(k))T_s \\ Fx(t), & (k + d(k))T_s \leqslant t < (k + 1)T_s \end{cases} \tag{8a}$$

$$v_o(t) = g^T x(t)\,, \tag{8b}$$

where V_s in (1) does not appear in (8a) since the input voltage has been chosen to coincide with the base voltage. The matrices F, f and g turn into

$$\begin{aligned} F &= 2\pi f_s \begin{bmatrix} -\frac{r_\ell}{x_\ell} & -\frac{1}{x_\ell} \\ r_o \frac{x_\ell - r_c r_\ell x_c}{(r_o + r_c) x_c x_\ell} & -\frac{x_\ell + r_c r_o x_c}{(r_o + r_c) x_c x_\ell} \end{bmatrix}, \\ f &= 2\pi f_s \begin{bmatrix} \frac{1}{x_\ell} \\ \frac{r_o}{r_o + r_c} \frac{r_c}{x_\ell} \end{bmatrix}, \qquad g = \begin{bmatrix} 0 & 1 \end{bmatrix}^T, \end{aligned} \tag{9}$$

using the normalized physical quantities to calculate their entries. The relation for the normalized output voltage error is given by

$$v_{o,err}(k) = \frac{1}{T_s} \int_{kT_s}^{(k+1)T_s} (v_o(t) - v_{o,ref})\, dt \tag{10}$$

with the normalized output voltage reference $v_{o,ref} = \frac{V_{o,ref}}{V_s}$. Furthermore, we use the base current I_b defined in the Appendix to normalize the current limit to

$$i_{\ell,max} = \frac{I_{\ell,max}}{I_b}\,. \tag{11}$$

Strictly speaking the converter model (8), which is normalized with respect to the input voltage, holds only for piecewise constant V_s. For the prediction model to be valid, one only needs to assume that the input voltage remains constant within the limited time of the prediction interval (a few switching periods). Since in practice the input voltage is either piecewise constant or varies only slowly compared to the (very short) switching period, the normalized state equations can serve as a sufficiently accurate prediction model.

Before proceeding, we elaborate on the parameters of the normalized and reformulated model. For the controller design, we assume that r_c, r_ℓ, x_ℓ and x_c are constant. Moreover, we assume that the load resistance r_o is constant[2], too, but the input voltage V_s may vary with time. Since the normalization renders the prediction model equations independent of (the time-varying) V_s, the matrices F, f and g in (9) are time-invariant. Hence,

[1]In general, such a substitution is not advisable, since the output voltage of most dc-dc converters is not continuous over time. For the step-down converter treated here, however, the output voltage is a continuous function of time.

[2]In Section IV-C, we will relax this assumption and introduce a Kalman filter to account for (unmeasured) changes in r_o.

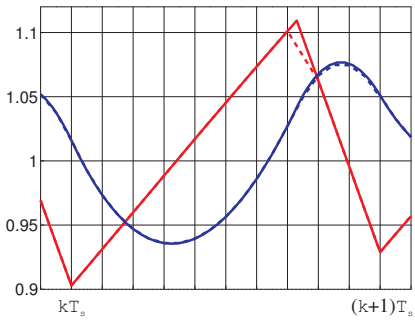

(a) The state evolution of the continuous-time nonlinear model (solid lines) compared with the sequence of states of the discrete-time hybrid model (dashed lines) using $\nu = 10$ subperiods, where the saw tooth shaped line represents i_ℓ and the smooth curve is v_c

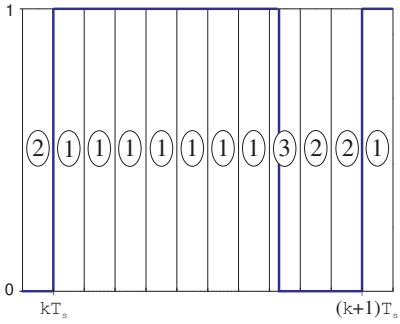

(b) Position of the switch S_1 and the mode active in the respective subperiod

Fig. 2: The ν-resolution modelling approach visualized for the k-th period

the only time-varying model parameters are the normalized output voltage reference $v_{o,ref}$ and the normalized current limit $i_{\ell,max}$.

B. ν-Resolution Discrete-Time Hybrid Model

Using the normalized and reformulated continuous-time model derived in the previous section as a starting point, the goal of this section is to derive a model of the converter that is suitable to serve as a prediction model for the optimal control problem formulation. This model should have the following properties. First, it is natural to formulate the model and the controller in the discrete-time domain, as the manipulated variable given by the duty cycle is constant within the switching period and changes only at the time-instants kT_s, $k \in \mathbb{N}_0$. Second, it would be beneficial to capture the evolution of the states also within the switching period, as this would enable us to impose constraints on the states not only at time-instants kT_s but also on intermediate samples. This is needed to keep the peaks of the inductor current below the current limit. Third, the model needs to yield an approximation of the output voltage error given by the integral (10).

Hereafter, we introduce the ν-resolution modelling approach that accounts for all the above requested properties. As illustrated in Fig. 2, the basic idea is to divide the period of length T_s into ν *notional subperiods* of length $\tau_s = T_s/\nu$ with $\nu \in \mathbb{N}$, $\nu \geq 1$. Within the k-th period, we use $\xi(n)$ to denote the states at time-instants $kT_s + n\tau_s$ with $n \in \{0, 1, \ldots, \nu\}$. Furthermore, by definition, $\xi(0) = x(k)$ and $\xi(\nu) = x(k+1)$ hold.

We would like to stress that the controller samples the physical plant only every T_s. Subdividing T_s into subperiods does *not* imply a higher sampling rate. The ν-resolution approach increases the model accuracy beyond standard averaging while retaining the sampling interval T_s.

For each subperiod, we introduce the two modes of operation discussed above (switch closed and open, respectively) plus an additional third (auxiliary) mode that captures the transition from mode one to mode two. More specifically, the modes are (i) the switch S_1 remains closed for the whole subperiod, (ii) the switch S_1 is open for the whole subperiod, and (iii) the switch S_1 is opening within the subperiod. Hence, for the n-th

subperiod, the state-update equation is

$$\xi(n+1) = \begin{cases} \Phi\ \xi(n) + \Psi, & d(k) \geq \frac{n+1}{\nu} \\ \Phi\ \xi(n), & d(k) < \frac{n}{\nu} \\ \Phi\ \xi(n) + \Psi(\nu d(k) - n), & \frac{n}{\nu} \leq d(k) < \frac{n+1}{\nu}\,, \end{cases} \tag{12}$$

where Φ and Ψ are the discrete-time representations of F and f as defined in (9) with "sampling" time τ_s. Note that if the third mode is active, i.e. $\frac{n}{\nu} \leq d(k) < \frac{n+1}{\nu}$ holds, $\nu d(k) - n$ is bounded by zero and one. Thus, the third mode is a weighted average of the modes one and two.

The safety current limit is imposed on the evolution of the states $\xi(n)$ by adding the constraints

$$-i_{\ell,max} \leq [1\ 0]\ \xi(n) \leq i_{\ell,max}, \quad n = 0, 1, \ldots, \nu - 1\,. \tag{13}$$

The notion of the ν-resolution modelling thus allows us to impose the current limit on the states $\xi(n)$ with the fine resolution $\frac{T_s}{\nu}$ rather than only on the states $x(k)$ with the coarse resolution T_s.

Using the output voltage given by

$$v_o(n) = g^T \xi(n)\,, \tag{14}$$

we approximate the voltage error integral (10) for the k-th period in the following way.

$$v_{o,err}(k) = \sum_{n=0}^{\nu-1} \frac{v_o(n) + v_o(n+1)}{2\nu} - v_{o,ref} \tag{15}$$

Before proceeding, we define constraints on the states, the parameters and the duty cycle. For the states, we require $x \in \mathcal{X}$, and the parameter vector $v_p = [v_{o,ref}\ \ i_{\ell,max}]^T$ is restricted to $v_p \in \mathcal{V}$, where $\mathcal{V}$ is application specific. The duty cycle, on the other hand, is physically restricted to $d \in \mathcal{U} = [0, 1]$.

In summary, the ν-resolution modelling approach provides a description of the state evolution within one period. In particular, the discrete-time sequence $[\xi(0), \xi(1), \ldots, \xi(\nu)]$ is an accurate representation of the continuous-time evolution of $x(t)$ for $t \in [kT_s, (k+1)T_s]$. The only approximation introduced is the weighted average that appears in the third mode of (12) when switch S_1 is turned off. By increasing ν the error introduced by averaging can be made arbitrarily small. This adds to the model complexity, but does not affect the sampling rate.

C. Formulation of ν-Resolution Model in PWA Form

For the computation of the state-feedback control law, the converter model is required to be in piecewise affine (PWA) form. Polyhedral PWA systems are defined by partitioning the state-input space into polyhedra and associating with each polyhedron an affine state-update and output function [21].

Starting from $\xi(0) = x(k)$ the discrete-time state-update map of the PWA model can be easily derived by using (12) consecutively for $n \in \{0, 1, \ldots, \nu - 1\}$ up to $x(k+1) = \xi(\nu)$. This state-update function maps the sampled state $x(k)$ from time-instant kT_s to time-instant $(k+1)T_s$. As an example for $\nu = 2$ this is

$$\begin{aligned} x(k+1) &= \Phi^2 x(k) + \\ &+ \begin{cases} 2\Phi\Psi d(k), & d(k) \in [0, \frac{1}{2}] \\ \Phi\Psi + 2\Psi(d(k) - \frac{1}{2}), & d(k) \in [\frac{1}{2}, 1] \end{cases}, \end{aligned} \tag{16}$$

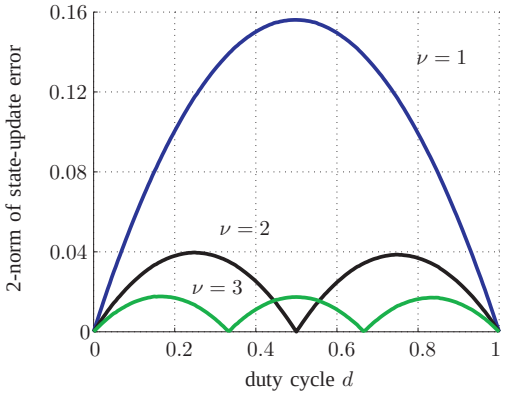

Fig. 3: Accuracy (2-norm error) of the state-update function of the ν-resolution model with respect to the nonlinear dynamics

where the matrices Φ and Ψ are derived by exact time-discretization over the subperiod $\tau_s = \frac{T_s}{2}$, i.e. $\Phi = e^{F\tau_s}$ and $\Psi = \int_0^{\tau_s} e^{F(\tau_s - t)} dt\, f$.

Since the converter dynamics are linear in the states, there is no partitioning in the state-space. Yet, they are nonlinear in the duty cycle. The ν-resolution model approximates this nonlinearity by partitioning the duty cycle in ν segments and by averaging the transition from the first to the second mode by a third (auxiliary) mode.

Using (12) in a similar way the current limit (13) and the output function (15) are computed. Obviously, (13) and (15) only depend on the state vector and duty cycle at time-instant kT_s.

D. Analysis of ν-Resolution Hybrid Model

For the set of converter parameters in Table I, Fig. 3 shows the accuracy of the state-update function of the ν-resolution model with respect to the nonlinear dynamics given by

$$x(k+1) = e^{FT_s} x(k) + \int_0^{d(k)T_s} e^{F(T_s - t)} dt\, f\,, \tag{17}$$

which is the exact discrete-time mapping from time-instant kT_s to $(k+1)T_s$. Specifically, the 2-norm (sum of squares) of the state-update error is plotted as a function of the duty cycle for $\nu = 1, 2, 3$. For $\nu = 2$ this error is given by the difference between (16) and (17). As the error is independent of the state $x(k)$, this comparison holds for the whole state-space.

The choice of $\nu = 1$ yields the standard (discrete-time) averaged model, which is predominately used for the controller design of dc-dc converters.

$$x(k+1) = \Phi\, x(k) + \Psi\, d(k) \tag{18}$$

with $\Phi = e^{FT_s}$ and $\Psi = \int_0^{T_s} e^{F(T_s - t)} dt\, f$. Obviously, the averaged model is perfectly accurate for $d(k) = 0$ and $d(k) = 1$, and it is at its worst for $d(k) = 0.5$. As one can see, setting ν to 2 significantly improves the accuracy of the model.

Note that the hybrid model is continuous in the states and input. This follows from the state-update equation (16) and is confirmed by the continuity in Fig. 3. Moreover, we would like to stress once more that the

ν-resolution model represents an accurate approximation of the nonlinear discrete-time dynamics (17) for all operating points, rather than being valid only locally for a specific operating point, as standard linearization would do. The trade-off between model accuracy and complexity is determined by the design parameter ν.

IV. Constrained Optimal Control

In this section, we propose a new constrained optimal control scheme for dc-dc converters. Such a controller can be considered as an extension of the Linear Quadratic Regulator to PWA systems. The controller derivation is done in three steps. First, an objective function is formulated. Second, an optimal state-feedback control law is derived, which minimizes the objective function subject to the evolution of the nominal ν-resolution model (nominal load $r_o = 1$ p.u.) and the constraints. In a last step, the controller is augmented by a Kalman filter, which adds an effective way to address unmeasured changes in the load resistor.

As stated earlier, we assume that the input and output voltages V_s and V_o, respectively, and the inductor current I_ℓ can be measured. The output reference voltage $V_{o,ref}$ and the current limit $I_{\ell,max}$ are given by the problem setup. Based on those measurements and parameters, the normalized quantities v_o, $v_{o,ref}$, i_ℓ and $i_{\ell,max}$, which will be used as the inputs to the optimal controller, directly follow[3].

A. Objective Function

The control objectives are to regulate the average output voltage to its reference as fast and with as little overshoot as possible, or equivalently, to (i) minimize the output voltage error $v_{o,err}$ (ii) despite changes in the input voltage V_s or changes in the load resistance r_o, and (iii) to respect the constraints on the inductor current and the duty cycle. For now, we assume that the load resistance r_o is time-invariant and nominal. We will drop this assumption in Section IV-C.

To induce a steady state operation under a constant non-zero duty cycle, we introduce the difference between two consecutive duty cycles

$$\Delta d(k) = d(k) - d(k-1)\,. \tag{19}$$

Next, we define the penalty matrix $Q = \text{diag}(q_1, q_2)$ with $q_1, q_2 \in \mathbb{R}^+$ and the vector $\varepsilon(k) = [v_{o,err}(k)\ \Delta d(k)]^T$ with $v_{o,err}(k)$ as defined in (15). We combine the (measured) state $x(k)$, the last control input $d(k-1)$, the output voltage reference $v_{o,ref}(k)$ and the current limit $i_{\ell,max}(k)$ into the parameter vector

$$p(k) = [(x(k))^T\ d(k-1)\ v_{o,ref}(k)\ i_{\ell,max}(k)]^T\,, \tag{20}$$

where $x \in \mathcal{X} \in \mathbb{R}^2$, $d \in \mathcal{U} = [0,1]$ and $[v_{o,ref}\ i_{\ell,max}]^T \in \mathcal{V} \in \mathbb{R}^2$. Consider the objective function

$$J(p(k), D(k)) = \sum_{\ell=0}^{N-1} \|Q\ \varepsilon(k+\ell|k)\|_1\,, \tag{21}$$

which penalizes the predicted evolution of $\varepsilon(k+\ell|k)$ from time-instant kT_s on over the finite horizon N using the 1-norm (sum of absolute values). Note that the objective function not only depends on the sequence of

[3]Since the circuit parameters are normalized over the time-varying input voltage V_s, the gains used for normalization are also time-varying and need to be recalculated at the beginning of each switching period, when a new measurement of V_s is acquired.

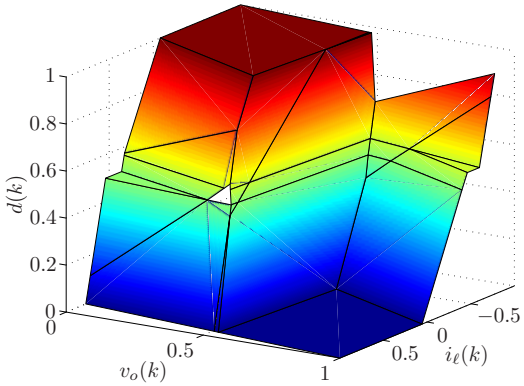

Fig. 4: State-feedback control law $d(k)$ for $d(k-1) = 0.67$, $v_{o,ref} = 0.6$ p.u. and $i_{\ell,max} = 0.89$ p.u., where dark blue corresponds to $d(k) = 0$ and dark red to $d(k) = 1$

control inputs $D(k) = [d(k), \ldots, d(k+N-1)]^T$ and the (measured) state $x(k)$, but also on the last control input $d(k-1)$, the output voltage reference $v_{o,ref}(k)$ and the current limit $i_{\ell,max}(k)$, which are allowed to be time-varying to account for changes in the input voltage $V_s(k)$.

Summing up, objective (i) is incorporated in the objective function, whereas objective (ii) is handled by normalizing the prediction model by V_s, feeding the model with $v_{o,ref}$, and adding in a later stage a Kalman filter. Objective (iii) is easily accounted for in the prediction model, where hard constraints are imposed on the inductor current and the duty cycle.

B. Constrained Optimal Control

At time-step kT_s the constrained optimal control problem is the following. Given the so called parameter vector $p(k)$ defined in (20), minimize the objective function (21) over the sequence of control inputs $D(k)$ subject to the evolution of the ν-resolution model in PWA form (e.g. (16)), the constraints on the sequence of duty cycles

$$0 \leq d(\ell) \leq 1\,, \quad \ell = k, ..., k+N-1\,, \tag{22}$$

similar constraints on the inductor current and the expression (19). The solution of this control problem can be pre-computed off-line for all $p \in \mathcal{X} \times \mathcal{U} \times \mathcal{V}$. To do so, we use the algorithm described in [22], where the solution is generated by combining dynamic programming with multi-parametric programming and some basic polyhedral manipulations. The resulting optimal state-feedback control law is a PWA function of $p(k)$ defined on a polyhedral partition of the five-dimensional parameter-space $\mathcal{X} \times \mathcal{U} \times \mathcal{V}$. More specifically, the parameter-space is partitioned into polyhedral sets and for each of these sets the optimal control law is given as an affine function of the parameter vector, which includes the state. For more details concerning the algorithm, the properties of its solution and computational tools the reader is referred to [23].

Example 1: Consider a step-down converter with the parameters given in Table I. Let the corresponding ν-resolution model (in PWA form) with $\nu = 2$ be defined on the set $\mathcal{X} = [-4, 4] \times [-0.1, 1]$ p.u., $\mathcal{U} = [0, 1]$ and $\mathcal{V} = [0.05, 1] \times [0, 3]$ p.u.. Then, for the control problem parameters given in Table I, we compute the PWA

state-feedback control law using the Multi-Parametric Toolbox [24]. The resulting controller is defined on 103 polyhedral regions in the five-dimensional parameter-space $\mathcal{X} \times \mathcal{U} \times \mathcal{V}$. Using the optimal complexity reduction algorithm [25], the controller is simplified to 50 regions.

To visualize the state-feedback control law, we substitute $v_{o,ref} = 0.6\,\text{p.u.}$ and $i_{\ell,max} = 0.89\,\text{p.u.}$ into the control law. As a result, the control law, which refers now to the nominal case, is defined on the three-dimensional space $\mathcal{X} \times \mathcal{U}$. Fig. 4 depicts the control input $d(k)$ as a PWA function of $x(k)$, where we additionally set $d(k-1) = 0.67$. Note that the control law is well-defined, that is for each $x(k) \in \mathcal{X}$ and $d(k-1) \in \mathcal{U}$ there exists a polyhedron and an associated affine control law such that $d(k)$ can be evaluated.

This control law, which is essentially a collection of (affine) P-controllers, can be interpreted as follows. In a small neighborhood of the steady state operating point, which is given by $i_\ell = 0.566\,\text{p.u.}$, $v_o = 0.5976\,\text{p.u.}$ and $d(k) = 0.67$, the controller resembles an affine P-controller. Further away from the operating point the behavior of the controller changes drastically. In particular, the control law saturates to respect the $[0, 1]$ constraint on the duty cycle and achieve optimality with respect to the objective function (21). For very low (very high) output voltages, in the region where the upper (lower) current constraint becomes active, the control law renders a very small (or even zero) duty cycle in order to avoid its violation. This is reflected in the "bending" of the control law visible in Fig. 4.

As is to be expected, the constrained optimal controller resembles the behavior of the existing traditionally designed PI-type control schemes including a current limit (and possibly also an anti-windup scheme). This is because the control objectives are the same in both cases. The major difference, however, is the validity of the controller for all operating points and the direct design procedure. This is in contrast to the (traditional) linear controller design that is valid only for a specific operating point.

C. Load Variations

In the following, we drop the assumption that the load resistance is known and time-invariant. To provide offset-free tracking of the output voltage reference despite unknown variations in the load, a loop is added. Specifically, the previously derived state-feedback controller (for a time-invariant and nominal load) is augmented by an external estimation loop that provides state estimates and also adjusts the normalized output voltage reference such that the error between the output voltage and its *actual* reference is made small.

Although such a voltage reference manipulation can be (and is conventionally) achieved by just adding an external PI loop, we opt in this paper for the use of a discrete-time Kalman filter [26] that yields a zero steady-state output voltage error due to its integrating character. The advantage of the employed approach is that with the Kalman filter no special anti-windup structure (the design of which would again depend on the operating point and on the expected load and set point changes) for handling the possible saturation of the related signals is required. In accordance with [27], the PWA model of the converter is augmented by two integrating disturbance states i_e and v_e that are used to model the effect of the changing load resistance on the inductor current and the output voltage respectively. The Kalman filter is used to estimate the augmented state vector

$$x_a = \begin{bmatrix} i_\ell & v_o & i_e & v_e \end{bmatrix}^T, \tag{23}$$

based on the measurements of i_ℓ and v_o. For the case $\nu = 2$ considered in this paper, the augmented model has the switched stochastic discrete-time state equations

$$\begin{aligned} x_a(k+1) &= \Phi_a^2 x_a(k) + G w_1(k) + \\ &+ \begin{cases} 2\Phi_a \Psi_a d(k), & d(k) \in [0, \frac{1}{2}] \\ \Phi_a \Psi_a + 2\Psi_a (d(k) - \frac{1}{2}), & d(k) \in [\frac{1}{2}, 1] \end{cases} , \end{aligned} \tag{24}$$

and the measurement equation

$$\begin{bmatrix} i_\ell(k) \\ v_o(k) \end{bmatrix} = C_a x_a(k) + H w_2(k) \,, \tag{25}$$

with

$$\Phi_a = \begin{bmatrix} \Phi & 0 \\ 0 & H \end{bmatrix}, \; \Psi_a = \begin{bmatrix} \Psi \\ 0 \\ 0 \end{bmatrix} , \tag{26}$$

$$C_a = \begin{bmatrix} 1 & 0 & 1 & 0 \\ 0 & 1 & 0 & 1 \end{bmatrix} ,$$

and $G = \text{diag}(1,1,1,1)$ and $H = \text{diag}(1,1)$. The random variables $w_1(k) \in \mathbb{R}^4$ and $w_2(k) \in \mathbb{R}^2$ represent the process and the measurement noise, respectively, with normal (Gaussian) probability distributions of covariance $E[w_1 w_1^T] = W_1$, $E[w_2 w_2^T] = W_2$ satisfying $G W_1 G^T \succeq 0$ and $W_2 + H W_1 H^T \succ 0$. The augmented model is detectable and uses the nominal value of the load resistor.

To address the hybrid nature of the model, a discrete-time Kalman filter with the same number of modes as the augmented PWA model of the converter is employed. Switching between the modes is trivial since the active mode of the PWA model (and hence of the Kalman filter) is imposed by the duty cycle and is therefore precisely known. For each mode the Kalman gain is constant, and since the state-update, the measurement and the covariance matrices are the same for all modes, it is trivial to show that the Kalman gains are the same, too. Therefore, only a single Kalman gain K needs to be computed and implemented.

The dynamic of the estimated state $\hat{x}_a(k)$ is described by

$$\begin{aligned} \hat{x}_a(k+1) &= \Phi_a^2 \hat{x}_a(k) + K C_a (x_a(k) - \hat{x}_a(k)) \\ &+ \begin{cases} 2\Phi_a \Psi_a d(k), & d(k) \in [0, \frac{1}{2}] \\ \Phi_a \Psi_a + 2\Psi_a (d(k) - \frac{1}{2}), & d(k) \in [\frac{1}{2}, 1] \end{cases} . \end{aligned} \tag{27}$$

To calculate the Kalman gain, the noise covariances matrices W_1 and W_2 are chosen such that high credibility is assigned to the measurements and dynamics of the physical states, namely i_ℓ and v_o, while low credibility is assigned to the dynamics of the disturbance states i_e and v_e. As a result, the Kalman filter provides estimates of the "slow" disturbances that can in turn be used to remove their influence from the output voltage. This is achieved by using the estimates of the states as inputs to the controller, while at the same time adjusting the output voltage reference $v_{o,ref}$ by the estimate of the corresponding disturbance state $\hat{v}_e$

$$\tilde{v}_{o,ref} = v_{o,ref} - \hat{v}_e \,. \tag{28}$$

Converter parameters			
in S.I.		*in p.u.*	
L	1 mH	x_ℓ	14.12 p.u.
C	220 μF	x_c	246.1 p.u.
R_c	0.5 Ω	r_c	0.0562 p.u.
R_ℓ	1.5 Ω	r_ℓ	0.1685 p.u.
R_o	8.9 Ω *(nominal)*	r_o	1 p.u. *(nominal)*
$I_{\ell,max}$	1 A	$i_{\ell,max}$	0.89 p.u. *(nominal)*
V_s	12 V *(nominal)*	v_s	1 p.u. *(nominal)*
$V_{o,ref}$	6 V	$v_{o,ref}$	0.6 p.u. *(nominal)*
Controller parameters			
ν	2	N	2
q_1	4	q_2	0.1
f_s	20 kHz		

TABLE I: Converter and controller parameters of the experimental results, where the parasitics are approximated values only

Moreover, since the controller uses the inductor current estimated by the Kalman filter, which equals the sum of the actual current i_ℓ and of the estimated disturbance $\hat{i}_e$, we also update the current limit constraint accordingly

$$\tilde{\hat{i}}_{\ell,max} = i_{\ell,max} - \hat{i}_e \,. \tag{29}$$

V. Experimental Results

In this section, experimental results demonstrating the potential advantages of the proposed control methodology are presented. Specifically, we examine the closed-loop dynamical behavior for the start-up, and the response to step changes in the input voltage and the load resistance, respectively.

The experimental setup was built using commercial electronic components – specifically, the switching stage comprises a IRF620 MOSFET and RURP1560 fast diode. The circuit parameters of the converter are summarized in Table I. If not stated otherwise, the input voltage is $V_s = 10\,\text{V}$ and the load resistance is given by $R_o = 8.9\,\Omega$. The output voltage reference is $V_{o,ref} = 6\,\text{V}$. The switching frequency is set to 20 kHz corresponding to a sampling interval of $50\,\mu$s.

The constrained optimal controller was implemented on a dSPACE$^{\text{TM}}$ DS1103 PPC controller board, where dSPACE allowed the development of the control software in a MATLAB/SIMULINK environment. Access to the I/O of the real-time hardware was obtained through Real Time Workshop blocks, allowing for a flexible and quick controller implementation. To protect the dSPACE$^{\text{TM}}$ controller board, a TLP2200 photo-coupler was used to electrically separate the controller from the dc-dc converter power circuit, and an IR2118 driver switched the MOSFET on or off. The inductor current measurement was obtained with a Hall effect transducer.

The ν-resolution model uses the same parameters as the physical plant model, with the difference that it is normalized with respect to V_s and that it always uses the nominal load $r_o = 1\,\text{p.u.}$. The choice of $\nu = 2$

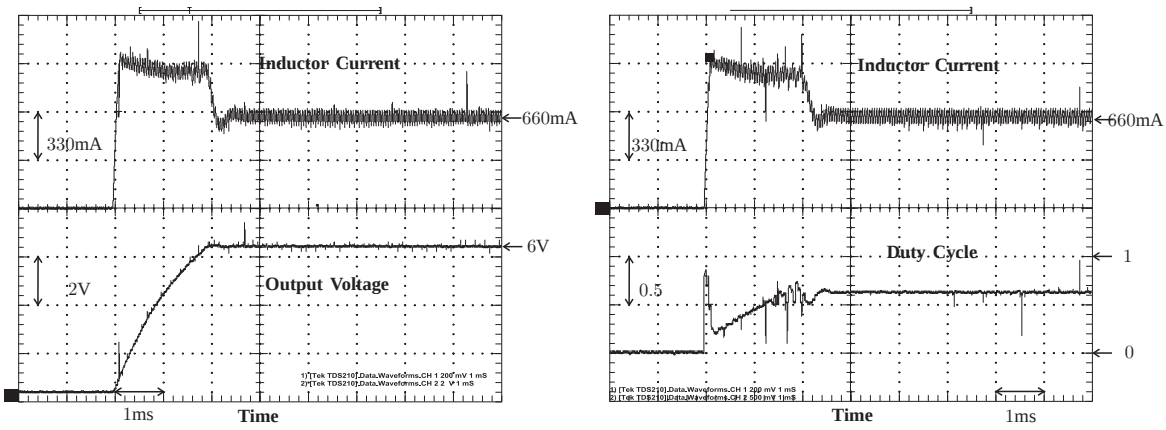

(a) Inductor current and output voltage

(b) Inductor current and duty cycle

Fig. 5: Experimental results for nominal start-up from initial condition zero

subperiods leads to a ν-resolution model that captures the nonlinear discrete-time dynamics in a sufficiently accurate way.

Regarding the optimal control scheme, the penalty matrix is chosen to be $Q = \text{diag}(4, 0.1)$, putting a rather small weight on the changes of the manipulated variable[4]. For all experiments, the prediction horizon is set to $N = 2$. Based on this, as detailed in Example 1, the PWA state-feedback control law shown in Fig. 4 is derived.

For the covariance matrices of the Kalman filter, we set $W_1 = \text{diag}(0.1, 0.1, 100, 100)$ and $W_2 = \text{diag}(1, 1)$.

A. Nominal Start-Up

Fig. 5(a) shows the inductor current and the output voltage of the converter in nominal operation ($R_o = 8.9\,\Omega$, $V_{o,ref} = 6\,\text{V}$) during start-up from zero as initial condition. As can be seen, the controller increases the current until the current limit is reached to charge the capacitor to the reference voltage level as fast as possible. Once the output voltage reaches its reference, the controller quickly restores the current to its nominal value to avoid any overshoot in V_o. For the same experiment (in a different instance), one can observe in Fig. 5(b) the evolution of the duty cycle, paired with the inductor current to allow for a direct comparison.

B. Step Changes in Input Voltage

Initially, the converter is operating at steady state with the input voltage $V_s = 16\,\text{V}$ when a ramp down to $V_s = 10\,\text{V}$ is applied. This disturbance is measured and fed to the controller at the beginning of the next switching period. The response of the converter is shown in Fig. 6, where one can see two different instances of the same experiment. Fig. 6(a) depicts the waveforms of the output voltage and the input voltage ramp,

[4]The penalty matrix determines the trade-off between the output voltage error and the controller effort (changes in the duty cycle). Hence, only the ratio between the diagonal elements is of importance. A ratio of 40 yields small output voltage errors with limited control effort. Ratios in the range of 30 to 60 yield very similar results.

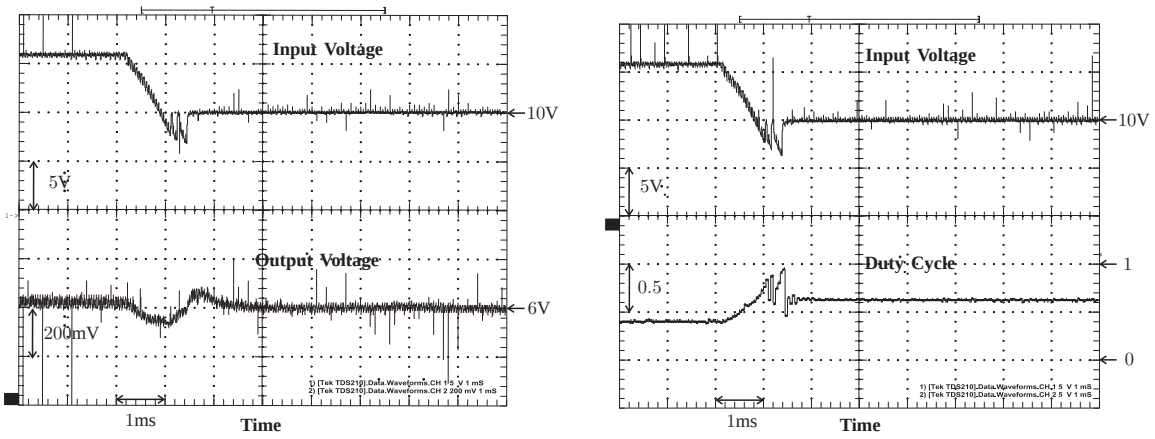

(a) Input voltage and output voltage

(b) Input voltage and duty cycle

Fig. 6: Experimental results for a ramp change in the input voltage from $V_s = 16\,\mathrm{V}$ to $V_s = 10\,\mathrm{V}$ within roughly $1\,\mathrm{ms}$

while Fig. 6(b) shows the controller action. The output voltage remains practically unaffected and the controller settles very quickly at the new steady-state duty cycle.

As can be seen, disturbances in the input voltage are rejected very effectively by the controller, and the output voltage is quickly restored to its reference. This is because the state-feedback control law is indirectly parameterized by the input voltage by normalizing the measured states, the output voltage reference and the current limit with respect to V_s. As a result, the performance of the controller is not affected by changes in V_s.

C. Step Changes in Load Resistance

In a last step, we investigate the closed-loop performance in the presence of major step changes in the load resistance. Starting from the nominal load $R_o = 8.9\,\Omega$, step changes to $R_o = 15\,\Omega$ and $R_o = 4\,\Omega$ are applied. As in the experiments above, the ν-resolution model and the state-feedback control law are designed assuming nominal load conditions. Yet, in the sequel, the Kalman filter is added to adjust the output voltage reference $v_{o,ref}$ accordingly.

Fig. 7 depicts the closed-loop performance of the converter for the step-up case. As can be observed, steady-state operation without a steady-state error in the output voltage is achieved due to the Kalman filter's inherent integrating action. Moreover, the converter response exhibits a relatively small overshoot.

In the last case, we examine a crucial aspect of the controller operation, namely the system's protection against excessive load currents, by applying a load drop from nominal to $R_o = 4\,\Omega$ chosen to activate the current limiting constraint of the controller. The experimental results in Fig. 8 show that the controller respects the current limit and forces the output voltage V_o to drop to the level needed to respect the constraint.

Even though such a current limiting protection scheme is present in all practical implementations, it is not directly treated as part of the controller design, but the current limit is imposed through an additional current loop. The proposed approach addresses the current constraint (as well as the duty cycle constraint) explicitly during the controller design.

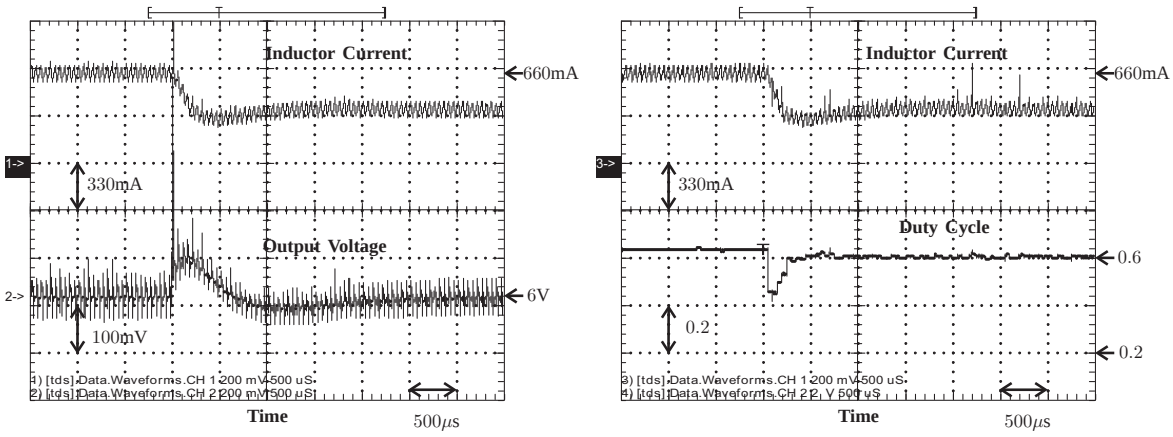

(a) Inductor current and output voltage

(b) Inductor current and duty cycle

Fig. 7: Experimental results for a step-up change in the load resistance from $R_o = 8.9\,\Omega$ to $R_o = 15\,\Omega$

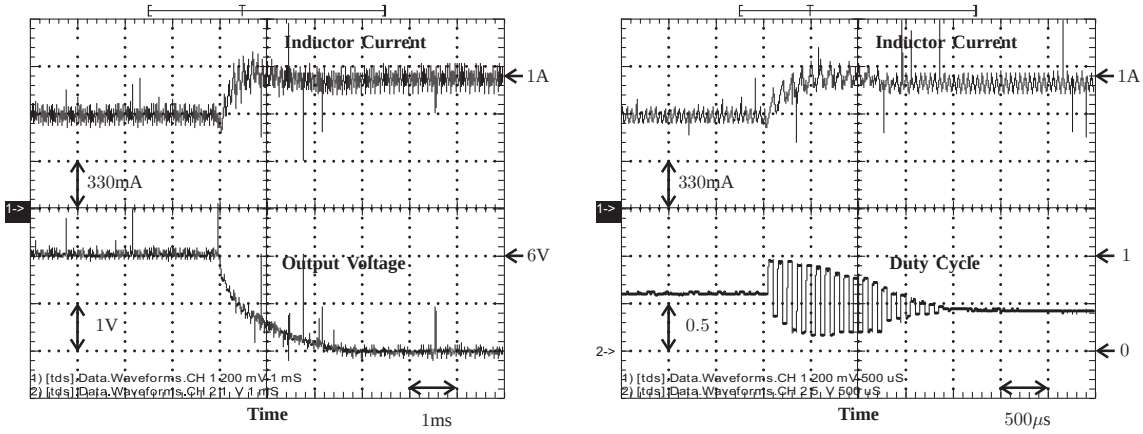

(a) Inductor current and output voltage

(b) Inductor current and duty cycle

Fig. 8: Experimental results for a drop in the load resistance from $R_o = 8.9\,\Omega$ to $R_o = 4\,\Omega$ showing the activation of the current limit constraint

Due to space limitations we do not provide here an elaborate comparison between the constrained optimal controller and traditional control techniques. Such a comparison is available from [28], where the performance of a constrained optimal controller is compared to the one achieved by a classic peak current mode control scheme.

Regarding the robustness of the constrained optimal control scheme with respect to model uncertainty, further to the evidence provided by the experimental results, simulation studies have shown that the proposed scheme can handle large variations in the converter parameters, without any significant performance deterioration. Although such studies cannot be presented here in any detail, the reader is referred to [29], where the MATLAB simulation files used for the development and evaluation of our controller are available for downloading and testing of the system behavior.

VI. Conclusions

We have presented a new modelling and control approach for fixed frequency switch-mode dc-dc converters by formulating a constrained optimal control problem using hybrid systems methodologies. The method is presented here for the synchronous step-down dc-dc converter, but as shown in [30], [31] and [32], it is directly extendable to other converter topologies including the boost and the buck-boost converter.

More specifically, a novel ν-resolution hybrid model was introduced to avoid averaging and to model the converter in an arbitrarily accurate way, and a constrained finite time optimal control problem was formulated and solved. This control methodology allowed us to explicitly take into account during the design phase physical constraints, such as the restriction of the duty cycle between zero and one, and safety constraints, such as current limiting. The resulting PWA state-feedback controller defined on a polyhedral partition of the parameter-space facilitates the practical implementation of the proposed scheme since it is nothing else but a very effective look-up table.

This controller is parameterized not only by the measured and normalized states $i_\ell(k)$ and $v_o(k)$, and the previous duty cycle $d(k-1)$, but also by the normalized output voltage reference $v_{o,ref}(k)$ and the normalized current limit $i_{\ell,max}(k)$. This allowed us to efficiently reject disturbances in the input voltage of any magnitude. Moreover, the addition of a Kalman filter estimating the output voltage error and adjusting the voltage reference accordingly provides disturbance rejection to large changes in the load resistance. These include low load resistances, for which the output voltage is dropped such that the safety constraint is respected. Experimental results have been provided demonstrating that the proposed controller leads to a closed-loop system with favorable dynamical properties – in particular during start-up and transients. Moreover, as shown in [10], exponential stability for the nominal closed-loop system can be proven by deriving a piecewise quadratic Lyapunov function.

Even though the control law computation and analysis relies on several algorithms and extensive computations, the derivation is greatly simplified by the Multi-Parametric Toolbox [24] that provides a unified framework for the modelling, synthesis and analysis of hybrid systems. All computational tools needed to reproduce the results shown in this paper are contained in this toolbox, and the MATLAB files for setting up and simulating the dc-dc converter can be downloaded from [29].

VII. Acknowledgements

This work was supported by the two European Commission research projects IST-2001-33520 *Control and Computation (CC)* and FP6-IST-511368 *Hybrid Control (HYCON)*.

References

[1] R. D. Middlebrook and S. Čuk, "A general unified approach to modeling switching power converter stages," in *Proc. IEEE Power Electron. Specialists Conf.*, 1976, pp. 18–34.

[2] R. W. Erickson, S. Čuk, and R. D. Middlebrook, "Large signal modeling and analysis of switching regulators," in *Proc. IEEE Power Electron. Specialists Conf.*, 1982, pp. 240–250.

[3] T. Gupta, R. R. Boudreaux, R. M. Nelms, and J. Y. Hung, "Implementation of a fuzzy controller for DC-DC converters using an inexpensive 8-b microcontroller," *IEEE Trans. Ind. Electron.*, vol. 44, no. 5, pp. 661–669, Oct. 1997.

[4] F. Garofalo, P. Marino, S. Scala, and F. Vasca, "Control of DC/DC converters with linear optimal feedback and nonlinear feedforward," *IEEE Trans. Power Electron.*, vol. 9, no. 6, pp. 607–615, Nov. 1994.

[5] H. Sira-Ramírez, "Nonlinear P-I controller design for switchmode DC-to-DC power converters," *IEEE Trans. Circuits Syst. I*, vol. 38, no. 4, pp. 410–417, Apr. 1991.

[6] S. R. Sanders and G. C. Verghese, "Lyapunov-based control for switched power converters," *IEEE Trans. Power Electron.*, vol. 7, no. 1, pp. 17–23, Jan. 1992.

[7] S. Hiti and D. Borojevic, "Robust nonlinear control for the boost converter," *IEEE Trans. Power Electron.*, vol. 10, no. 6, pp. 651–658, Nov. 1995.

[8] M. K. Kazimierczuk and A. Massarini, "Feedforward control dynamic of DC/DC PWM boost converter," *IEEE Trans. Circuits Syst. I*, vol. 44, no. 2, pp. 143–149, Feb. 1997.

[9] M. K. Kazimierczuk and L. A. Starman, "Dynamic performance of PWM DC/DC boost converter with input voltage feedforward control," *IEEE Trans. Circuits Syst. I*, vol. 46, no. 12, pp. 1473–1481, Dec. 1999.

[10] T. Geyer, "Low complexity model predictive control in power electronics and power systems," Dr. sc. tech. thesis, Automatic Control Laboratory ETH Zurich, 2005.

[11] F. H. F. Leung, P. K. S. Tam, and C. K. Li, "The control of switching DC-DC converters – a general LQR problem," *IEEE Trans. Ind. Electron.*, vol. 38, no. 1, pp. 65–71, Feb. 1991.

[12] ——, "An improved LQR-based controller for switching DC-DC converters," *IEEE Trans. Ind. Electron.*, vol. 40, no. 5, pp. 521–528, Oct. 1993.

[13] M. Lazar and R. De Keyser, "Non-linear predictive control of a dc-to-dc converter," in *Symposium on Power Electronics, Electrical Drives, Automation and Motion*, Capri, Italy, 2004.

[14] D. W. Clarke, C. Mohtadi, and P. S. Tuffs, "Generalized predictive control – part I. The basic algorithm," *Automatica*, vol. 23, no. 2, pp. 137–148, 1987.

[15] S. Chattopadhyay and S. Das, "A digital current-mode control technique for dc-dc converters," *IEEE Trans. Power Electron.*, vol. 21, no. 6, pp. 1718–1726, Nov. 2006.

[16] G. Feng, E. Meyer, and Y. F. Liu, "A new digital control algorithm to achieve optimal dynamic performance in dc-to-dc converters," *IEEE Trans. Power Electron.*, vol. 22, no. 4, pp. 1489–1498, July 2007.

[17] D. M. Van de Sype, K. De Gussemé, F. M. L. L. De Belie, A. P. Van den Bossche, and J. A. Melkebeek, "Small-signal z-domain analysis of digitally controlled converters," *IEEE Trans. Power Electron.*, vol. 21, no. 2, pp. 470–478, Mar. 2006.

[18] H. Peng, A. Prodic, E. Alarcon, and E. Maksimovic, "Modeling of quantization effects in digitally controlled dc-dc converters," *IEEE Trans. Power Electron.*, vol. 22, no. 1, pp. 208–215, Jan. 2007.

[19] W. Stefanutti, P. Mattavelli, G. Spiazzi, and P. Tenti, "Digital control of single-phase power factor preregulators based on current and voltage sensing at switch terminals," *IEEE Trans. Power Electron.*, vol. 21, no. 5, pp. 1356–1363, Sept. 2006.

[20] D. P. Bertsekas, *Dynamic Programming and Optimal Control*. Athena Scientific, 1995.

[21] E. D. Sontag, "Nonlinear regulation: The piecewise linear approach," *IEEE Trans. Automat. Contr.*, vol. 26, no. 2, pp. 346–358, Apr. 1981.

[22] M. Baotić, F. J. Christophersen, and M. Morari, "A new algorithm for constrained finite time optimal control of hybrid systems with a linear performance index," in *Proc. of the European Control Conf.*, Cambridge, UK, Sept. 2003.

[23] F. Borrelli, M. Baotić, A. Bemporad, and M. Morari, "Dynamic programming for constrained optimal control of discrete-time linear hybrid systems," *Automatica*, vol. 41, no. 10, pp. 1709–1721, Oct. 2005.

[24] M. Kvasnica, P. Grieder, M. Baotić, and M. Morari, "Multi parametric toolbox (MPT)," in *Hybrid Systems: Computation and Control*, ser. LNCS, R. Alur and G. Pappas, Eds. Springer, 2004, vol. 2993, pp. 448–462, http://control.ee.ethz.ch/~mpt.

[25] T. Geyer, F. D. Torrisi, and M. Morari, "Optimal complexity reduction of piecewise affine models based on hyperplane arrangements," in *Proc. American Control Conf.*, Boston, MA, June 2004, pp. 1190–1195.

[26] A. H. Jazwinski, *Academic Press*. Stochastic Processes and Filtering Theory, 1970, vol. ethbib P712310:64.

[27] G. Pannocchia and J. B. Rawlings, "Disturbance models for offset-free model-predictive control," *Aiche J.*, vol. 49, no. 2, pp. 426–437, Feb. 2003.

[28] T. Geyer, G. Papafotiou, and M. Morari, "Hybrid model predictive control of the step-down dc-dc converter," Automatic Control Laboratory ETH Zurich, http://control.ee.ethz.ch, Tech. Rep. AUT08-01, 2008.

[29] G. Papafotiou, "Constrained optimal control of dc-dc converters," http://control.ee.ethz.ch/index.cgi?page=publications&action=details&id=2702, 2006.

[30] A. G. Beccuti, G. Papafotiou, and M. Morari, "Explicit model predictive control of the boost dc-dc converter," in *Proceedings of the 2nd IFAC Conf. on Analysis and Design of Hybrid Systems*, Alghero, Italy, 2006.

[31] ——, "Optimal control of the buck dc-dc converter operating in both the continuous and discontinuous conduction regimes," in *Proc. 45th IEEE Conf. on Decision and Control*, San Diego, California, USA, Dec. 2006.

[32] A. G. Beccuti, M. Lazar, W. P. G. H. Heemels, G. Papafotiou, and M. Morari, "Assessment of nonlinear predictive control techniques for dc-dc converters," in *Proceedings of the IFAC Nonlinear Control Design Symposium*, Pretoria, South Africa, 2007.

VIII. Appendix

To normalize the converter equations (1)–(7), the actual (time-varying) input voltage $V_s(k)$, the nominal (time-invariant) load resistance R_o and the (time-invariant) switching frequency f_s are used as base quantities. Setting $R_b = R_o$, one can deduce the base inductance and capacitance as

$$L_b = \frac{R_b}{2\pi f_s}\,, \quad C_b = \frac{1}{2\pi f_s R_b}\,, \tag{30}$$

respectively. The normalized values of the inductance and the capacitance of the converter are defined as

$$x_\ell = \frac{L}{L_b}\,, \quad x_c = \frac{C}{C_b}\,. \tag{31}$$

Similarly, the resistances of the circuit are normalized through

$$r_\ell = \frac{R_\ell}{R_b}\,, \quad r_c = \frac{R_c}{R_b}\,, \quad r_o = \frac{R_o}{R_b}\,. \tag{32}$$

Using the measured (and hence time-varying) input voltage $V_s(k)$ as base quantity, the (time-varying) base current at time-instant k follows as

$$I_b(k) = \frac{V_s(k)}{R_b} \tag{33}$$

leading to the normalized output voltage and inductor current

$$v_o(k) = \frac{V_o(k)}{V_s(k)}\,, \quad i_\ell(k) = \frac{I_\ell(k)}{I_b(k)}\,, \tag{34}$$

respectively.